Title

Snapshot transient absorption spectroscopy: toward in vivo investigations of nonphotochemical quenching mechanisms

Journal

Photosynthesis Research, 141(3)

ISSN

0166-8595

Authors

Park, Soomin
Steen, Collin J
Fischer, Alexandra L
et al.

Publication Date

2019-09-01

DOI

10.1007/s11120-019-00640-x

Peer reviewed

Snapshot transient absorption spectroscopy: toward in vivo investigations of nonphotochemical quenching mechanisms

Soomin Park[1,2,3] · Collin J. Steen[1,2,3] · Alexandra L. Fischer[1,2,3,4] · Graham R. Fleming[1,2,3]

Abstract

Although the importance of nonphotochemical quenching (NPQ) on photosynthetic biomass production and crop yields is well established, the in vivo operation of the individual mechanisms contributing to overall NPQ is still a matter of contro-versy. In order to investigate the timescale and activation dynamics of specific quenching mechanisms, we have developed a technique called snapshot transient absorption (TA) spectroscopy, which can monitor molecular species involved in the quenching response with a time resolution of 30 s. Using intact thylakoid membrane samples, we show how conventional TA kinetic and spectral analyses enable the determination of the appropriate wavelength and time delay for snapshot TA experi-ments. As an example, we show how the chlorophyll-carotenoid charge transfer and excitation energy transfer mechanisms can be monitored based on signals corresponding to the carotenoid (Car) radical cation and Car S_1 excited state absorption, respectively. The use of snapshot TA spectroscopy together with the previously reported fluorescence lifetime snapshot technique (Sylak-Glassman et al. in Photosynth Res 127:69–76, 2016) provides valuable information such as the concurrent appearance of specific quenching species and overall quenching of excited Chl. Furthermore, we show that the snapshot TA technique can be successfully applied to completely intact photosynthetic organisms such as live cells of *Nannochloropsis*. This demonstrates that the snapshot TA technique is a valuable method for tracking the dynamics of intact samples that evolve over time, such as the photosynthetic system in response to high-light exposure.

Introduction

Photosynthetic organisms must consistently balance efficient light harvesting and the need to avoid the harmful effects associated with absorbing too much light (Barber and Anderson 1992; Li et al. 2009). One such way that photosynthetic organisms minimize photooxidative damage is through the dissipation of excess absorbed light energy as heat, a process referred to as nonphotochemical quenching (NPQ). Technically, NPQ encompasses a suite of different processes that differ in the molecular species involved, in the timescales of their activation and subsequent relaxation, and possibly in their specific location within the chloroplast. The activation of NPQ decreases the lifetime of excited chlorophyll (Chl*), which in turn can make the formation of reactive oxygen species less probable. Energy-dependent quenching (qE) accounts for the majority (~75%) of the overall NPQ (Demmig-Adams et al. 1996) and is the most rapid component of the photoprotective response, becoming active within seconds to minutes of exposure to high light (Müller et al. 2001). A deeper knowledge of the underlying molecular mechanisms associated with qE is beneficial especially since it has recently been shown that regulating proteins involved in qE can improve water use efficiency (Głowacka et al. 2018) as well as increase biomass

Soomin Park and Collin J. Steen contributed equally to this work.

✉ Graham R. Fleming
grfleming@lbl.gov

[1] Department of Chemistry, University of California, Berkeley, CA 94720, USA

[2] Molecular Biophysics and Integrated Bioimaging Division, Lawrence Berkeley National Laboratory, Berkeley, CA 94720, USA

[3] Kavli Energy Nanoscience Institute, Berkeley, CA 94720, USA

[4] Present Address: Intel Corporation, NE Century Blvd 2501, Hillsboro, OR 97214, USA

productivity in algae (Berteotti et al. 2016) and green plants (Kromdijk et al. 2016) under fluctuating light conditions.

Despite the importance of qE to plant fitness and survival, its underlying mechanisms remain controversial or unknown. Several different mechanisms have been proposed including excitation energy transfer (EET) quenching in which energy is transferred from a Chl molecule to a carotenoid (Car) molecule followed by energy dissipation (Fig. 1a) (Ruban et al. 2007; Staleva et al. 2015; Liguori et al. 2017). Charge transfer (CT) quenching is also possible in which electron transfer from Car to Chl results in the formation of a dimer state which can accept energy from a neighboring Chl molecule (Fig. 1b) (Dreuw et al. 2003; Ahn et al. 2008). This is followed by charge recombination and rapid relaxation to the ground state, dissipating energy in the process. Other proposed mechanisms include an excitonic quenching model based on bidirectional energy transfer between Chl and Car (Bode et al. 2009) and Chl–Chl CT (Miloslavina et al. 2008; Müller et al. 2010). We note that it is possible that multiple mechanisms may be occurring simultaneously and that the given mechanisms may differ depending upon the overall protein (and chemical) environment.

However, these proposed mechanisms have been largely based on in vitro studies of isolated proteins, which cannot reflect normal physiological conditions. Recent studies have revealed that Car orientations (Liguori et al. 2017; Hontani et al. 2018), as well as various Car-Chl (Balevičius et al. 2017), Car-protein (Liguori et al. 2017), pigment-protein (Pascal et al. 2005; Wahadoszamen et al. 2014; Sacharz et al. 2017), and protein–protein interactions (Liguori et al. 2015) can control the dynamics of excitation energy in intact systems. As such, to obtain physiologically relevant information, it is necessary to perform experiments on systems that exist in a state as near native as possible. For example, previous transient absorption (TA) spectroscopy studies of crude thylakoid membranes from spinach and *Arabidopsis thaliana* have confirmed the presence of both EET (Ma et al. 2003) and CT (Holt et al. 2005) quenching based on the observation of Car S_1 and $Car^{\cdot+}$ excited state absorptions (ESA) after Chl excitation. However, it is still very challenging to obtain information on specific mechanisms in vivo because conventional TA measurements of intact samples (e.g., cells, leaves, and thylakoid membranes) are accompanied by large scattering, many spectrally overlapping signals, and a poor signal-to-noise ratio. For these reasons, it has not been possible to collect quantitative and dynamic information on the specific quenching mechanisms in intact samples.

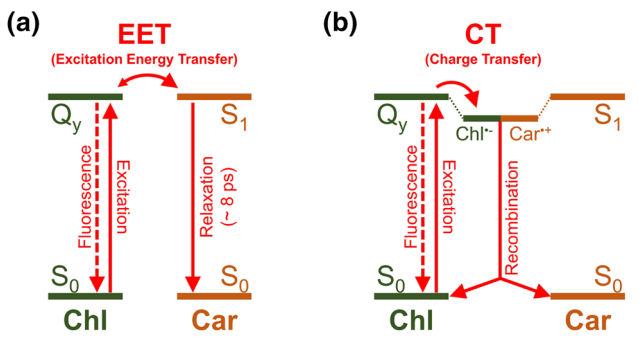

Fig. 1 Schematic energy-level diagrams illustrating the steps involved in the proposed excitation energy transfer (EET) and charge transfer (CT) quenching mechanisms involving Chl-Car interactions

To address these issues, we have developed an ultrafast spectroscopic technique called snapshot TA spectroscopy. Using this technique, snapshots that correspond to the ESA signal can be collected from intact thylakoid membranes or whole cells in 10 s windows at intervals ranging from 30 s to 1 min, which is adequate to resolve the timescale of qE. Consequently, snapshot TA allows us to not only observe the molecular species involved in the qE mechanisms, but also to monitor their participation as photosynthetic organisms experience changes in light intensity in real time.

In this paper, we introduce the snapshot TA technique and describe how it is a useful development for answering long-debated questions about the mechanism of NPQ in photosynthesis. Specifically, we describe the application of snapshot TA spectroscopy to monitor the Car S_1 and $Car^{\cdot+}$ signals as a photosynthetic sample is exposed to high light, which directly probes the in vivo operation of the Chl-Car EET and CT mechanisms, respectively. Furthermore, we present the activation and relaxation of the EET and CT mechanisms in the context of overall Chl* quenching by showing our snapshot TA data in conjunction with the Chl fluorescence lifetime snapshots, which are measured using the previously reported Chl fluorescence lifetimes snapshot technique (Sylak-Glassman et al. 2016).

Methods

Snapshot TA measurements were carried out using a similar procedure to that described by Park et al. (2017, 2018) (Fig. 2a). A Ti/sapphire regenerative amplifier (Coherent, RegA 9050) seeded by a Ti/sapphire oscillator (Coherent, MIRA Seed) and a diode-pumped laser (Coherent, Verdi V-18) was used to generate 800 nm pulses with a repetition rate of 250 kHz.

The 800 nm beam was split using a beam splitter. To generate the probe, the beam was focused on a 1 mm sapphire crystal or yttrium aluminum garnet (YAG) crystal to produce a visible continuum or a near infrared continuum, respectively. Following continuum generation, a 700-nm short-pass filter or a 850-nm long-pass filter was placed to filter out undesired wavelengths. To generate the pump, an optical parametric amplifier (Coherent, OPA 9450) was tuned to generate pulses centered at 650 or 665 nm for either the

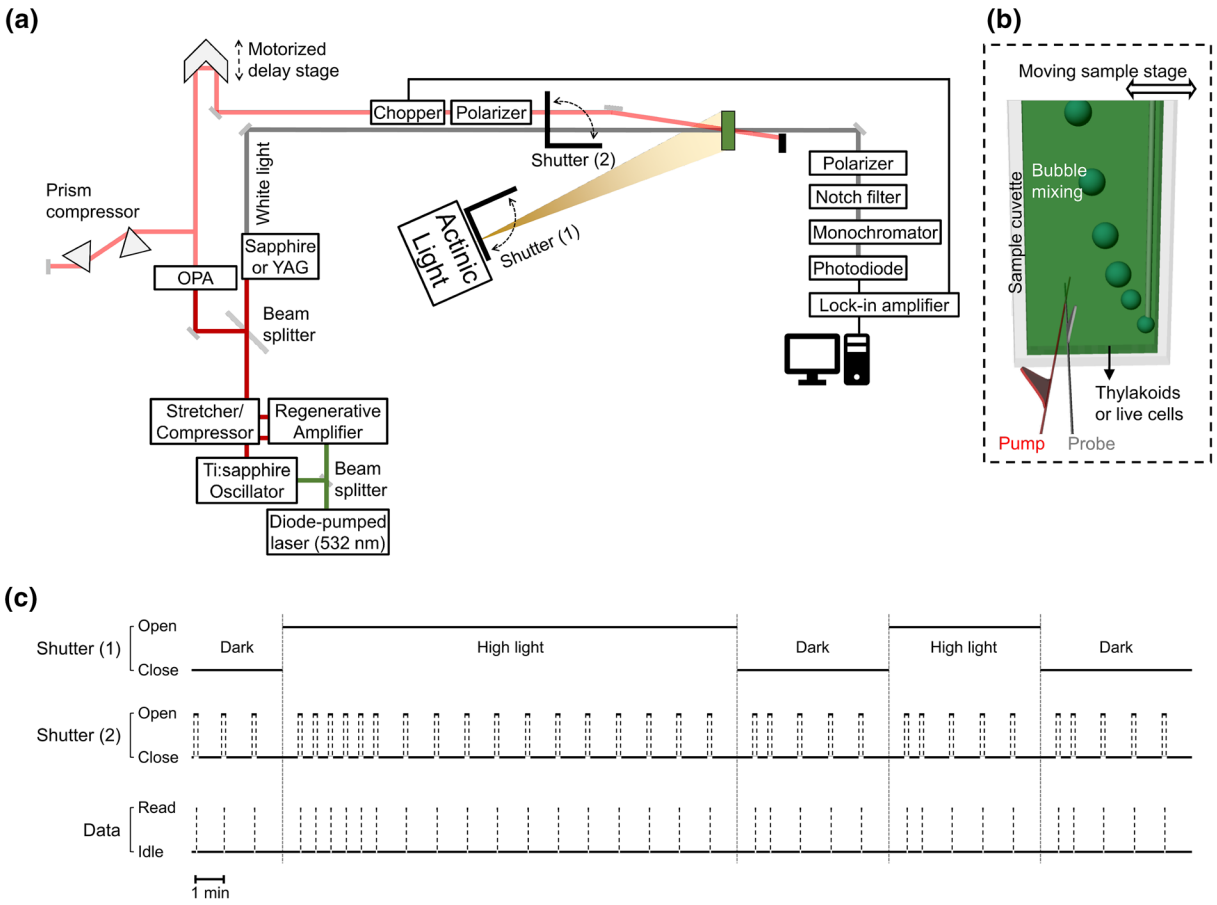

Fig. 2 Experimental setup and data acquisition sequence for snapshot transient absorption spectroscopy. **a** Block diagram of the laser utilized for snapshot TA spectroscopy. **b** Pictorial representation of the sample cell containing thylakoid membranes or live *N. oceanica* cells in a cuvette. **c** Schematic of the data acquisition process. Shutter 1 controls the exposure of the sample to an actinic light, while shutter 2 controls the exposure of the laser beams to the sample for data acquisition as described in main text

Chl *b* Q_y transition or the blue edge of the Chl *a* Q_y transition, respectively. The pump pulses had a FWHM of 50 fs. The pump and probe were 150 µm and 65 µm in diameter, respectively, and the beams were overlapped at the sample at the magic-angle (54.7°) polarization. At 540 nm, the cross-correlation time between the pump and probe was found to be ~ 120 fs. Another polarization filter set to the probe polarization and a 658 ± 26 nm notch filter were placed after the sample to minimize pump scattering and ensure a clean probe signal. The probe then passed through a monochromator (Acton Research Corp., SpectraPro 300i). The signal was detected using a Si-biased photodiode (Thorlabs, DET10A) connected to a lock-in amplifier (Stanford Research, SR830), which was synchronized to a chopper positioned in the pump beam path. For high-light exposure, an actinic light with a heat absorbing filter (KG1) was set to an intensity of 850 µmol photons·m^{-2} s^{-1} at the sample position.

To prepare crude thylakoid membranes, fresh spinach leaves were purchased from a local market the day before the measurements and stored in the dark at 4 °C overnight. Crude thylakoid membranes were isolated in a dark cold room (4 °C), using a procedure similar to that reported previously (Gilmore et al. 1998). The final concentration of all thylakoid samples was adjusted to 50–100 µg Chl/ml using reaction buffer immediately before the measurement (Porra et al. 1989). The reaction buffer contained 30 mM ascorbic acid, 0.5 mM ATP, and 50 µM methyl viologen at pH 8. For snapshot TA of *Nannochloropsis oceanica* microalgae, live cell sample solutions were prepared in Ficoll 400 buffer at a concentration of 40 mg Chl *a*/mL. For all experiments, the sample cuvette had a path length of 1 mm and was continuously translocated to prevent sample damage and accumulation of long-lived triplet Chl* state. Photodegradation is primarily dependent on the stability of the sample throughout exposure to the laser and actinic light. Spinach thylakoid membranes and intact cells of *N. oceanica* were found to be stable for at least 30 min of snapshot TA. Importantly, to further prevent sample agglomeration and precipitation, the sample solution was gently mixed by bubbling air between snapshot measurements (Fig. 2b).

A custom LabVIEW program was used for data collection. Each snapshot measurement was controlled by a shutter programmed to open for 10 s increments at various times throughout the exposure of a sample to high light or dark conditions, while the data was continuously collected by the lock-in amplifier. Further decreases in the duration of the data acquisition (below 10 s windows) is limited by the signal-to-noise (SN) ratio. Measurements of intact samples (e.g., thylakoid membranes and live algae cells), though physiologically relevant, exhibit high scattering and consequently poor SN ratio. This required us to use a rather intense pump laser (20–40 nJ/pulse), which can generate significant Chl*–Chl* annihilation and provide an additional Chl* de-excitation pathway beyond the naturally occurring NPQ mechanisms. For samples with very little scatter, it will be possible to decrease the snapshot time windows. It is also possible that a more sensitive detector (e.g., a photodiode and data acquisition card whose sampling clock is synchronized to the repetition rate of the laser (Werley et al. 2011)) could help to minimize annihilation processes by permitting the use of reduced pump power and increasing the temporal resolution (currently 10 s) of the snapshot TA system.

The specific actinic light and snapshot sequence used in our TA experiments is depicted in Fig. 2c. Snapshots were taken periodically throughout an initial 3 min dark period. Then, an actinic light with intensity 850 µmol photons m^{-2} s^{-1} was used to activate qE. The actinic light remained on for 15 min and snapshots were taken throughout this period. Following light exposure, snapshots were taken for 5 min in the dark to assess recovery from qE. A second cycle of 5 min periods of light and dark exposure was incorporated in order to assess the effect of dark recovery and subsequent re-exposure to quenching-inducing conditions.

As shown in Fig. 3, 15 data points can be collected during the 10 s time window between shutter open and close. Note that the number of data points collected within the time window can be controlled by adjusting the time constant of the lock-in amplifier. When shutter 2 opens, the signal transiently fluctuated due to the response time of the sensing system before stabilizing within a few seconds. In order to obtain reliable data and ensure that all PSII reaction centers are closed, we calculate the average of five data (dΔOD) points which were collected 5.5–8.5 s after the opening of the shutter.

Fluorescence lifetime snapshot measurements have been performed based on the previously reported method (Sylak-Glassman et al. 2016). The power of 420 nm excitation pulse was approximately 1.6 mW (21 pJ/pulse) at the sample. The amplitude-weighted average lifetime ($\tau_{average}$) is calculated using the following equation:

$$\tau_{average} = \frac{\sum_i A_i \tau_i}{\sum_i A_i} \quad (1)$$

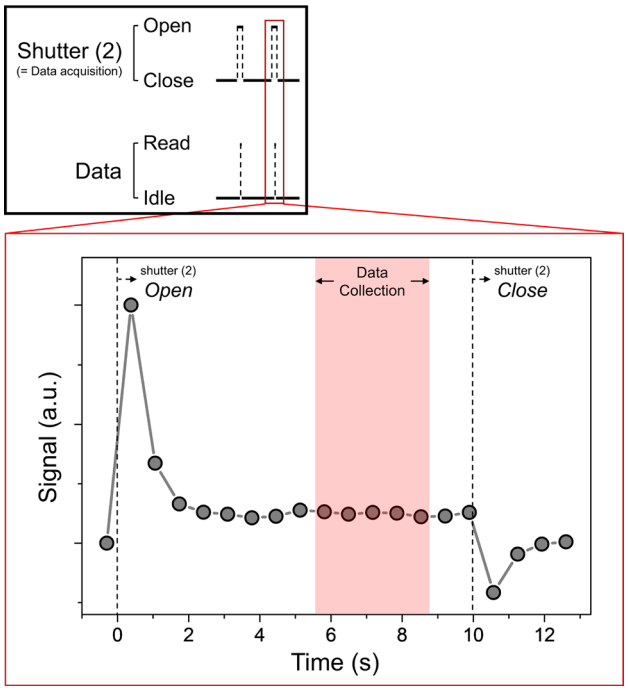

Fig. 3 Representative snapshot TA data measurement performed on spinach thylakoid membranes. Vertical lines correspond to the time at which the laser shutter was opened or closed. The red region corresponds to reliable measurements which were averaged to provide a single "snapshot" data point

where A_i and τ_i are the amplitudes and the fluorescence lifetime components, respectively, which is obtained from fitting the fluorescence decay with 3 exponentials. The NPQ response (NPQ_τ) in terms of the average florescence lifetime is defined as:

$$NPQ_\tau = \frac{\tau_{avg,dark} - \tau_{avg,light}}{\tau_{avg,light}} \quad (2)$$

where $\tau_{avg,dark}$ is the average of three lifetime snapshots measured during the initial dark period.

Results

Snapshot TA is a variation of conventional TA spectroscopy that utilizes a fixed time delay and wavelength in order to monitor slow changes (s to min timescale) in the dynamics of ultrafast processes (fs to ps timescale). Here, we focus on the detection of Car S_1 and $Car^{\cdot+}$ ESA signals via snapshot TA spectroscopy, thereby demonstrating its utility to monitor the EET and CT mechanisms in spinach thylakoid membranes and live cells of *Nannochloropsis oceanica*. First, the time delay and probe wavelength for snapshot TA experiments must be selected to correspond to the time delay and

wavelength associated with the absorption maximum in the TA kinetic profile and spectrum, respectively.

Figure 4 shows conventional TA kinetic profiles and reconstructed spectra of Car S_1 and $Car^{\cdot+}$ ESA measured in spinach thylakoid membranes after Chl excitation at 650 nm. The ESA signals at 540 nm in dark and high light were measured to evaluate the Car S_1 ESA. In high light, there is a decrease in the overall contribution of Chl *a* ESA in the visible region due to the activation of de-excitation pathways (NPQ, etc.) for the Chl Q_y excited state. However, the dark and high-light TA kinetic profiles exhibit nearly identical kinetics for time delays greater than 40 ps. In order to extract the contribution of only the Car S_1–S_N ESA from the overall profile, it is necessary to scale the dark profile to match the high-light profile at a time delay of 40 ps in order to remove the contribution of Chl *a* ESA. The scaling factor is simply the ratio between the OD at 40 ps in the light (ΔODat40 ps(t)) and dark (ΔODat40 ps(dark)). It should also be noted that the decrease in Chl *a* ESA upon high-light exposure is rather insignificant in the near IR; thus, no re-scaling is necessary for the Car radical cation signal (Fig. 4c). This scaling process is described in Fig. 4a and Table 1 of the manuscript. Therefore, for accurate kinetic analyses, precise determination of the background signal (dark signal) is important in order to assess the effect induced by high-light exposure. Our previous publications (Park et al. 2017, 2018) include similar snapshot TA data for spinach thylakoid membranes and above-mentioned data analyses.

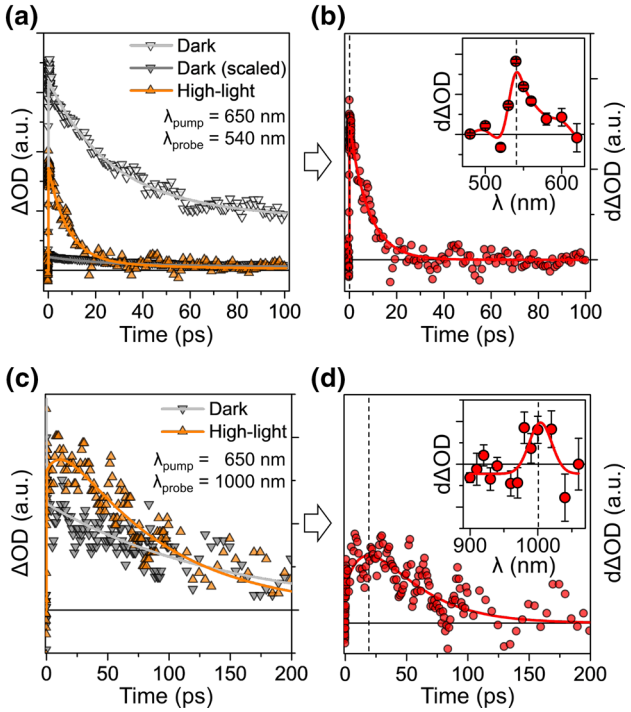

Fig. 4 TA kinetic profiles for spinach thylakoid membranes probed at 540 nm (**a**) and 1000 nm (**c**) under dark and high-light conditions, respectively. Note that the dark profile at 540 nm was re-scaled to account for the decrease in overall Chl ESA that occurs in the visible region upon high-light exposure. Difference TA kinetic profiles obtained by subtracting the dark kinetic profile from the high-light profile, which corresponds to Car S_1 ESA signal (**b**) and $Car^{\cdot+}$ ESA signal (**d**). The inset graph shows the difference TA spectra measured in the visible and near-IR regions. Dashed vertical lines indicate the specific time delay and wavelength selected for each snapshot TA measurements. Each data point is presented as the mean ± SE ($n = 5$)

The general form of equation for extracting snapshot TA signal (dΔOD) can be written as

$$\mathrm{dOD}_x(T) = \mathrm{dOD}_{\mathrm{at}t,\lambda}(T) - C \cdot \mathrm{dOD}_{\mathrm{at}t,\lambda}(T = 0)$$

where x is the excited-state species of interest (i.e., Car S_1), t and λ are the time delay and wavelength where the maximum signal was observed from conventional TA spectroscopy, respectively. T is the real time (time after high-light exposure) and C is the scaling factor, the ratio of amplitudes of background signals at $T = 0$ compared to T, which is used to remove the contribution of Chl *a* ESA as mentioned above.

Figure 4b shows difference (dΔOD) TA profiles, which were fitted well to a single exponential decay with a lifetime of 8.03 ± 0.40 ps, which is consistent with the characteristic

Table 1 Equations used to calculate Car S_1 and $Car^{\cdot+}$ ESA signals

Excited state	Equation	
Car S_1	$\mathrm{d\Delta OD}_{\mathrm{Car}S_1}(T) = \Delta\mathrm{OD}_{\mathrm{at1ps}}(T) - \Delta\mathrm{OD}_{\mathrm{at1ps}}(\mathrm{dark}) \times \left(\frac{\Delta\mathrm{OD}_{\mathrm{at40ps}}(T)}{\Delta OD_{\mathrm{at40ps}}(\mathrm{dark})}\right)$	
	Conditions	Selected wavelength/time delay: 540 nm/1 ps Car S_1 ESA at 40 ps ≅ 0 (Ma et al. 2003) $\Delta\mathrm{OD}_{\mathrm{at40ps}}$ (high light) < $\Delta\mathrm{OD}_{\mathrm{at40ps}}$ (dark) (Park et al. 2018)
$Car^{\cdot+}$	$\mathrm{d\Delta OD}_{\mathrm{Car}^{\cdot+}}(T) = \Delta\mathrm{OD}_{\mathrm{at20ps}}(T) - \Delta\mathrm{OD}_{\mathrm{at20ps}}(\mathrm{dark})$	
	Conditions	Selected wavelength/time delay: 1000 nm/20 ps Chl $\mathrm{ESA}_{\mathrm{at20ps}}$ (high light) ≅ Chl $\mathrm{ESA}_{\mathrm{at20ps}}$ (dark) (Holt et al. 2005; Park et al. 2017)

Note that $\Delta\mathrm{OD}_{\mathrm{at1ps}}$(T), $\Delta\mathrm{OD}_{\mathrm{at20ps}}$(T), and $\Delta\mathrm{OD}_{\mathrm{at40ps}}$(T) represent the snapshot TA signal measured at time delays of 1 ps, 20 ps, and 40 ps, respectively, over the course of light exposure. ΔOD(dark) is the average of TA signals measured during the initial dark period

decay time for the S_1 state of the carotenoid zeaxanthin (Zea). The spectrum of this difference TA signal (Fig. 4b, inset) closely resembles those reported in the literature for a Car S_1–S_N transition (Polívka and Sundström 2004). Additionally, this difference TA spectrum exhibits a peak at 540 nm which is slightly blue-shifted (~ 15 nm) from the Zea S_1–S_N absorption peak measured in methanol, likely due to differences attributed to the environment (protein vs. solvent) (Polívka and Sundström 2004). Finally, we have previously observed that treatment with DTT, an inhibitor of violaxanthin de-epoxidase (VDE), resulted in negligible accumulation of Zea and elimination of the Car S_1 ESA signal (Park et al. 2018), further suggesting that the specific carotenoid involved is zeaxanthin. Detailed information on the kinetics of this Car S_1 ESA signal will be discussed later. Based on these observations, snapshot measurements of the Car S_1 ESA signals were collected at a selected time delay of 1 ps and a wavelength of 540 nm.

Using a similar subtraction of dark and high-light kinetic profiles, the $Car^{\cdot+}$ ESA shows a characteristic rise ($\tau_{rise} = 19.2 \pm 13.7$ ps) and decay ($\tau_{decay} = 34.4 \pm 18.7$ ps) (Fig. 4c and d). For snapshot TA, we selected a time delay of 20 ps and a wavelength of 1000 nm because this is where the $Car^{\cdot+}$ ESA signal shows maximum absorption. Using these fixed time delays and wavelengths, the ESA signals were collected during the time sequence of actinic light on and off. The specific equations used to calculate Car S_1 and $Car^{\cdot+}$ ESA (dΔOD) and related assumptions are presented in Table 1.

Figure 5a shows the results of snapshot TA measurements on isolated spinach thylakoid membranes. The signals for both Car S_1 and $Car^{\cdot+}$ ESA clearly increase and decrease in response to high-light and dark exposure, suggesting that the EET (Chl $Q_y \rightarrow$ Car S_1) and CT ($Chl^{\cdot-}$–$Car^{\cdot+}$) mechanisms become active in the high-light-adapted state of spinach thylakoid membranes. Both signals rapidly increase and reach a maximum within 2 to 3 min of high-light exposure and quickly disappear within 5 min of subsequent dark exposure.

These snapshot TA results are well complemented by fluorescence lifetime snapshot measurements (Sylak-Glassman et al. 2016). Fluorescence lifetime snapshots provide direct information on the quenching of Chl* by monitoring the evolution of the fluorescence lifetime as intact samples adapt to high light. Fluorescence lifetimes are also independent of photobleaching and chloroplast movement, making them preferable to conventional PAM fluorescence. Figure 5b shows the results of fluorescence lifetime snapshots of spinach thylakoid membranes. Upon illumination, the average Chl fluorescence lifetime rapidly decreases from ~ 1.5 ns to ~ 0.3 ns, which is indicative of the activation of qE. Following 15 min of high light, the actinic light was turned off and the fluorescence lifetime increased to ~ 0.8 ns, reflecting recovery of qE. Subsequent light exposure results in another

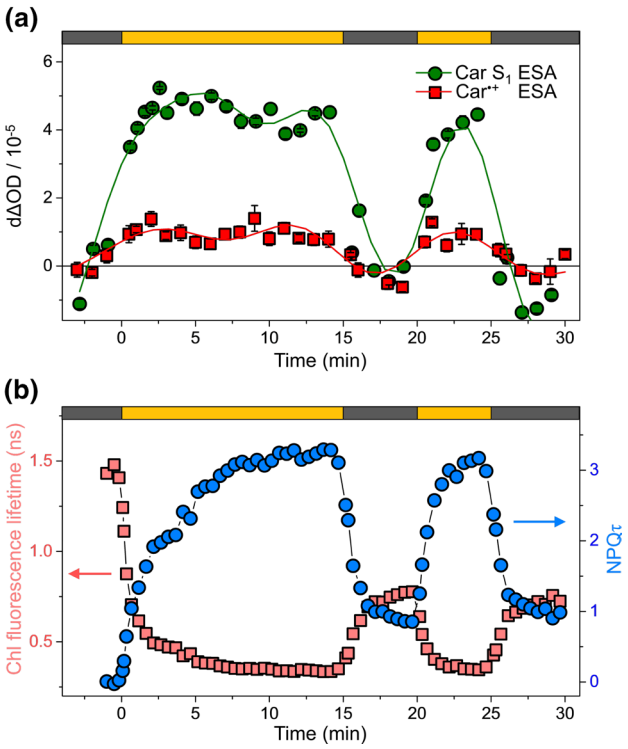

Fig. 5 TA and fluorescence lifetime snapshot results for spinach thylakoid membranes. **a** TA snapshots corresponding to the Car S_1 ESA and $Car^{\cdot+}$ ESA are shown in green circles and red squares, respectively. The probe wavelength was set to 540 and 1000 nm for the EET (Car S_1 ESA) and CT ($Car^{\cdot+}$ ESA) mechanisms, respectively. **b** Fluorescence lifetime snapshots (pink squares) and the corresponding NPQτ parameter (blue circles). The bars at the top of the panels indicate the time sequence of actinic light on (yellow) and off (dark gray)

decrease in the fluorescence lifetime. All of these changes in the fluorescence lifetime are contained in NPQ_τ (blue data points in Fig. 5b, see "Methods" section for the calculation), a lifetime-based parameter analogous to the conventional NPQ value ($NPQ = (F_m - F'_m)/F'_m$).

Fundamentally, fluorescence tells us that "energy goes away", but it provides no indication as to "where it goes". In this regard, snapshot TA is a valuable complement to the fluorescence lifetime snapshot technique. The combination of snapshot TA results and fluorescence lifetime snapshots (Fig. 5) can simultaneously show the appearance of the quenching species (i.e., Car S_1 and $Car^{\cdot+}$) in the overall context of Chl* quenching (i.e., Chl fluorescence lifetime). In spinach thylakoids, while the Car S_1 and $Car^{\cdot+}$ signals were at their maximum after 5 min of light exposure, 82% of the overall NPQ_τ was achieved. In the subsequent 5 min of dark exposure, both ESA signals rapidly disappeared while a 75% loss in the NPQ_τ level was observed. Moreover, the second period of high light generated a similar amplitude of both ESA signals. These observations suggest that the Chl-Car EET and CT mechanisms play a central role in rapidly

reversible qE and photoprotection under fluctuating light conditions. Note that both Car S_1 and $Car^{\cdot+}$ signals are zero in the second dark period, but the fluorescence lifetime is not fully recovered to the original dark-adapted value, suggesting a longer-lasting mechanism not signaled by absorptions at 540 nm or 1000 nm.

In the quantitative analysis of Car S_1 and $Car^{\cdot+}$ ESA snapshots and their correlation with Chl* quenching as determined by fluorescence, we face two main issues. First, precise molar extinction coefficients (ε) for the Car S_1–S_N and $Car^{\cdot+}$ D_0–D_2 transitions in the photosystem II (PSII) protein environment are unavailable. If the values for ε become available, the density of quenching traps could then be calculated and incorporated in quantitative models of qE (Amarnath et al. 2016; Bennett et al. 2018). The second issue is related to the process of annihilation, which is more prevalent within photosynthetic complexes at high pulse powers (Gulbinas et al. 1996; Barzda et al. 2001). Our snapshot TA measurements are taken at pump intensities ranging from 20 to 40 nJ/pulse. Given that the lifetime of the Chl ESA signal observed in the TA measurement is less than 0.1 ns (Fig. 4a), which is significantly lower than the Chl fluorescence lifetime (0.3–1.5 ns, Fig. 5b) measured under annihilation-free condition (21 pJ/pulse), it seems obvious that annihilation significantly affects the dynamics of excitation energy transfer. As discussed below, this difference makes it difficult to directly correlate the appearance of quenching species observed from snapshot TA with the degree of Chl* quenching quantified by Chl fluorescence lifetime snapshot measurements.

For example, under annihilation-free (natural) conditions, the rate of excitation energy transfer via diffusion ($k_{\text{diffusion}} \cong (350\ \text{ps})^{-1}$; see details in Table 2) is significantly slower than that of de-excitation by EET quenching ($k_{\text{EETquenching}} \cong (8\ \text{ps})^{-1}$; see details in Table 2). This fast quenching rate results in negligible population of the Car S_1 excited states (Fig. 6a) (Polívka and Sundström 2004). However, in our TA measurement, the diffusion length for excitation energy becomes significantly restricted due to the presence of annihilation, which apparently acts as a strong Chl* quenching pathway (Barzda et al. 2001). Consequently, only energy residing on Chl pigments that are very close to a Car molecule can populate the Car excited states. In other words, we can only observe the populated Car S_1 state and corresponding ESA signal presented in Fig. 4b under conditions

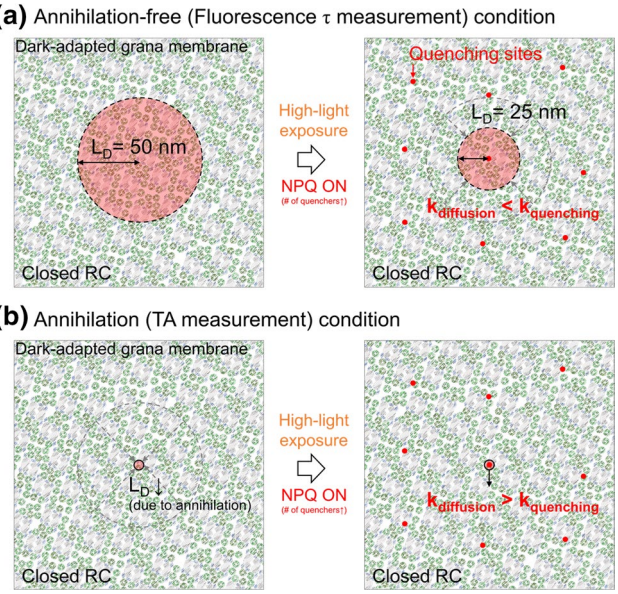

Fig. 6 Proposed scheme showing the excitation diffusion length (L_D, red circles) in dark and high-light-exposed grana membranes when all reaction centers (RCs) are closed. **a** Under annihilation-free conditions, such as the pulse powers used in fluorescence lifetime snapshots, the diffusion lengths were estimated based on the recently developed multiscale model (Bennett et al. 2018) and our Chl fluorescence lifetime snapshot data (Fig. 5b). In response to high-light exposure, the appearance of quenching sites (red dots) decreases the diffusion length to 25 nm which corresponds to NPQ ≅ 3, according to the empirical relationship between the NPQ parameter and L_D shown in Bennett et al. (2018). Under this condition, the rate of excitation diffusion is less than that of quenching, resulting in the case where excited states of the quencher are hardly populated. **b** Intense pump powers, such as those used in the snapshot TA measurements, can result in significant annihilation. This results in a dramatic decrease in the excitation diffusion length regardless of the presence of quenchers. If the reduced diffusion length is small enough, the rate of diffusion becomes faster than the rate of quenching. In this case, we can observe both the rapid population of the excited states of the quenching species as well as the subsequent relaxation process

Table 2 Estimated rate constants of excitation diffusion and de-excitation by quenching

Process	Rate constant	Experimental basis	Reference
Excitation diffusion	$k_{\text{diffusion}} \cong (350\ \text{ps})^{-1}$	Chl fluorescence lifetime ($\tau \sim 350$ ps) of quenched thylakoids under annihilation-free condition	This study (Fig. 5b) Park et al. (2017, 2018)
EET quenching	$k_{\text{EETquenching}} \cong (8\ \text{ps})^{-1}$	S_1 lifetime of carotenoid Zea ($\tau_{\text{decay}} \sim 8$ ps)	This study (Fig. 4b) Ma et al. (2003) Park et al. (2018)
CT quenching	$k_{\text{CTquenching}} = (40\ \text{ps})^{-1}$ to $(150\ \text{ps})^{-1}$	Lifetime of Car radical cation ($\tau_{\text{decay}} = 40$–150 ps)	This study (Fig. 4d) Holt et al. (2005) Park et al. (2017)

where annihilation is active. The lack of rise time for the Car S_1 ESA signal in Fig. 4b indicates that the Car S_1 state is instantaneously (≤ 120 fs) populated after Chl excitation, which is possible only if $k_{diffusion} > k_{EETquenching}$ (Fig. 6b). Interestingly, in the case of the Chl-Car CT state ($Car^{\cdot+}$ ESA) we were able to observe an increasing population of the CT state with a rise time of ~ 20 ps. This difference is likely attributed to the slower $Chl^{\cdot+}$–$Car^{\cdot+}$ charge recombination process (≤ $(40\ ps)^{-1}$; see details in Table 2) relative to Car S_1 relaxation. Therefore, to draw more quantitative information (e.g., the densities of EET and CT quenching sites) from our snapshot TA data, the relative speeds of excitation diffusion and quenching in addition to the effect of annihilation on Chl* dynamics need to be considered when developing a quantitative qE model such as Bennett et al. 2018. Once annihilation is incorporated into the model, we will be able to accurately simulate the natural dynamics of excitation energy transport in intact grana membranes based on the appearance and disappearance of EET and CT quenching sites as determined from TA spectroscopy.

While we have thus far focused on snapshot TA investigations of isolated thylakoid membranes, the technique can also be applied to completely in vivo systems. As an in vivo proof-of-concept study, we performed snapshot Car S_1 ESA TA measurements on live cells of an alga, *Nannochloropis oceanica*. *N. oceanica* appears to be an ideal sample for snapshot TA given that is smaller (2–3 μm) than other model algae (Vieler et al. 2012) and it possesses a simple pigment composition (Llansola-Portoles et al. 2017). These factors result in suppressed pump scattering and less spectrally overlapping signals, respectively. Figure 7 shows the results of in vivo TA and snapshot TA spectroscopy and the corresponding Chl fluorescence lifetime snapshots. Since *N. oceanica* does not contain the carotenoid lutein, zeaxanthin is the most probable Chl* quencher. In fact, a knock-out mutant of violaxanthin de-epoxidase (VDE), an enzyme that is responsible for the accumulation of Zea in response to high light, lacks most of the qE capabilities of wild-type *N. oceanica* (Park et al. 2019). The Car (Zea) S_1 ESA signal extracted by subtracting the dark signal from the high-light signal (Fig. 7a) was fitted well with a single exponential decay ($\tau_{decay} = 7.71 \pm 1.34$ ps), which is almost identical to the decay of the Car S_1 ESA observed in spinach thylakoid membranes.

Interestingly, it appears that the Car (Zea) S_1 snapshots in *N. oceanica* correlate well with the onset of overall quenching as evidenced by the NPQτ values calculated from fluorescence lifetime snapshots (Fig. 7c), suggesting that EET is one of the mechanisms that is responsible for qE activation. While NPQτ decreases upon returning to the dark, the Car (Zea) S_1 signals slightly decrease (Fig. 7c). This observation could indicate that the decrease of EET mechanism is also involved in the relaxation of qE in *N. oceanica*. We recently discovered that this EET mechanism as well as the CT mechanism is controlled by two important proteins (Park et al. 2019).

Concluding remarks

Although NPQ processes are routinely assessed by measuring the reduced amount or lifetime of Chl fluorescence, which is a downstream effect of quenching, the complexity of NPQ mechanisms and their ensemble effect make it infeasible to characterize individual quenching mechanisms and understand the design principles of such mechanisms under in vivo conditions. By monitoring the Car S_1 and $Car^{\cdot+}$ ESA in real time as intact samples adapt to high light, it

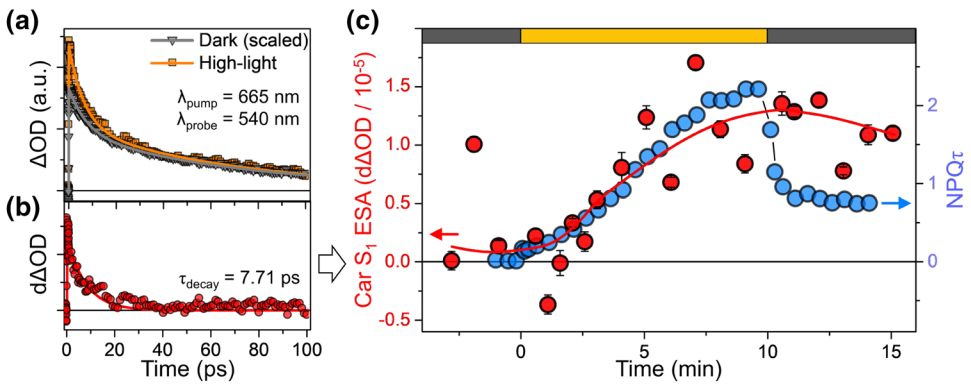

Fig. 7 TA spectroscopic studies of *N. oceanica* live cells. **a** TA kinetic profiles under dark and high-light conditions. The probe wavelength was set to 540 nm for the EET (Car S_1 ESA) quenching mechanism. **b** Difference TA kinetic profile ($\tau_{decay} = 7.71 \pm 1.34$ ps) obtained by subtracting the scaled dark kinetic profile from the high-light profile. **c** TA and Chl fluorescence lifetime snapshots for *N. oceanica* live cells. The TA snapshots corresponding to the Car S_1 ESA are depicted by red circles. Each data point is presented as the mean ± SE ($n = 5$). The NPQτ values (blue circles) were calculated from Chl fluorescence lifetime snapshots using Eq. 2. The bars at the top of the panels indicate the time sequence of actinic light on (yellow) and off (dark gray)

is possible to observe the timescale and activation dynamics of the Chl-Car EET and CT mechanisms. Using similar measurements to those described here along with known chemical inhibitors of important qE players (e.g., PsbS, VDE), we were able to observe the EET and CT quenching mechanisms in spinach thylakoid membranes, each of which is triggered by different processes (Park et al. 2017, 2018). By recording quantitative and dynamic signals of the indi-vidual quenching mechanisms and combining the data with fluorescence lifetime snapshots (Sylak-Glassman et al. 2016) performed on the same intact samples, we are able to provide a broader picture of the overall excitation quenching mecha-nisms that are so essential to plant fitness and crop yields.

Our studies have focused exclusively on the temporal response of the photosynthetic apparatus to high-light exposure, but the snapshot TA technique is potentially valuable for tracking the excited state population and dynamics within any sample that changes over time. Some examples of this include tracking processes such as in situ thin-film formation for photovoltaic applications (Hernandez et al. 2015; Wilson and Wong 2018) and degradation of perovskites by moisture/O_2 (Wang et al. 2015; Ginting et al. 2017).

Acknowledgements We thank Drs. Dagmar Lyska and Masakazu Iwai for helpful discussions and for providing *Nannochloropsis oceanica* samples. We also thank Lam Lam for helpful assistance during her visit to the University of California, Berkeley. This work was supported by the U.S. Department of Energy, Office of Science, Basic Energy Sciences, Chemical Sciences, Geosciences, and Biosciences Division under Field Work Proposal 449B. G. R. F. thanks Magdalen College, Oxford for a visiting Fellowship, and the Department of Physical and Theoretical Chemistry, Oxford for their hospitality during the writing of this paper.

Compliance with ethical standards

Conflict of interest The authors declare that they have no conflict of interest.

References

Ahn TK, Avenson TJ, Ballottari M et al (2008) Architecture of a charge-transfer state regulating light harvesting in a plant antenna protein. Science 320:794–797. https://doi.org/10.1126/science.1154800

Amarnath K, Bennett DIG, Schneider AR, Fleming GR (2016) Multiscale model of light harvesting by photosystem II in plants. Proc Natl Acad Sci USA 113:1156–1161. https://doi.org/10.1073/pnas.1524999113

Balevičius V, Fox KF, Bricker WP et al (2017) Fine control of chlorophyll-carotenoid interactions defines the functionality of light-harvesting proteins in plants. Sci Rep 7:1–10. https://doi.org/10.1038/s41598-017-13720-6

Barber J, Anderson B (1992) Too much of a good thing: light can be bad for photosynthesis. Trends Biochem Sci 17:61–66. https://doi.org/10.1016/0968-0004(92)90503-2

Barzda V, Gulbinas V, Kananavicius R et al (2001) Singlet-singlet annihilation kinetics in aggregates and trimers of LHCII. Biophys J 80:2409–2421

Bennett DIG, Fleming GR, Amarnath K (2018) Energy-dependent quenching adjusts the excitation diffusion length to regulate photosynthetic light harvesting. Proc Natl Acad Sci USA. https://doi.org/10.1073/pnas.1806597115

Berteotti S, Ballottari M, Bassi R (2016) Increased biomass productivity in green algae by tuning non-photochemical quenching. Sci Rep 6:21339. https://doi.org/10.1038/srep21339

Bode S, Quentmeier CC, Liao P-N et al (2009) On the regulation of photosynthesis by excitonic interactions between carotenoids and chlorophylls. Proc Natl Acad Sci USA 106:12311–12316. https://doi.org/10.1073/pnas.0903536106

Demmig-Adams B, Adams WW III, Barker DH et al (1996) Using chlorophyll fluorescence to assess the fraction of absorbed light allocated to thermal dissipation of excess excitation. Physiol Plant 98:253–264

Dreuw A, Fleming GR, Head-Gordon M (2003) Charge-transfer state as a possible signature of a zeaxanthin-chlorophyll dimer in the non-photochemical quenching process in green plants. J Phys Chem B 107:6500–6503. https://doi.org/10.1021/jp034562r

Gilmore AM, Shinkarev VP, Hazlett TL, Govindjee (1998) Quantitative analysis of the effects of intrathylakoid pH and xanthophyll cycle pigments on chlorophyll a fluorescence lifetime distributions and intensity in thylakoids. Biochemistry 37:13582–13593. https://doi.org/10.1021/bi981384x

Ginting RT, Jeon MK, Lee KJ et al (2017) Degradation mechanism of planar-perovskite solar cells: correlating evolution of iodine distribution and photocurrent hysteresis. J Mater Chem A 5:4527–4534. https://doi.org/10.1039/c6ta09202k

Głowacka K, Kromdijk J, Kucera K et al (2018) Photosystem II Subunit S overexpression increases the efficiency of water use in a field-grown crop. Nat Commun 9:868. https://doi.org/10.1038/s41467-018-03231-x

Gulbinas V, Valkunas L, Kuciauskas D et al (1996) Singlet-singlet annihilation and local heating in FMO complexes. J Phys Chem 100:17950–17956. https://doi.org/10.1021/jp961272k

Hernandez JL, Reichmanis E, Reynolds JR (2015) Probing film solidification dynamics in polymer photovoltaics. Org Electron Phys Mater Appl 25:57–65. https://doi.org/10.1016/j.orgel.2015.05.025

Holt NE, Zigmantas D, Valkunas L et al (2005) Carotenoid cation formation and the regulation of photosynthetic light harvesting. Science 307:433–436. https://doi.org/10.1126/science.1105833

Hontani Y, Kloz M, Polívka T et al (2018) Molecular origin of photoprotection in cyanobacteria probed by watermarked femtosecond stimulated Raman spectroscopy. J Phys Chem Lett 9:1788–1792. https://doi.org/10.1021/acs.jpclett.8b00663

Kromdijk J, Glowacka K, Leonelli L et al (2016) Improving photosynthesis and crop productivity by accelerating recovery from photoprotection. Science 354:857–862

Li Z, Wakao S, Fischer BB, Niyogi KK (2009) Sensing and responding to excess light. Annu Rev Plant Biol 60:239–260. https://doi.org/10.1146/annurev.arplant.58.032806.103844

Liguori N, Periole X, Marrink SJ, Croce R (2015) From light-harvesting to photoprotection: structural basis of the dynamic switch of the major antenna complex of plants (LHCII). Sci Rep 5:15661. https://doi.org/10.1038/srep15661

Liguori N, Xu P, van Stokkum IHM et al (2017) Different carotenoid conformations have distinct functions in light-harvesting regulation in plants. Nat Commun 8:1994. https://doi.org/10.1038/s41467-017-02239-z

Llansola-Portoles MJ, Litvin R, Ilioaia C et al (2017) Pigment structure in the violaxanthin–chlorophyll-a-binding protein VCP. Photosynth Res 134:51–58. https://doi.org/10.1007/s11120-017-0407-6

Ma Y-Z, Holt NE, Li X-P et al (2003) Evidence for direct carotenoid involvement in the regulation of photosynthetic light harvesting. Proc Natl Acad Sci USA 100:4377–4382. https://doi.org/10.1073/pnas.0736959100

Miloslavina Y, Wehner A, Lambrev PH et al (2008) Far-red fluorescence: a direct spectroscopic marker for LHCII oligomer formation in non-photochemical quenching. FEBS Lett 582:3625–3631. https://doi.org/10.1016/j.febslet.2008.09.044

Müller P, Li X-P, Niyogi KK (2001) Non-photochemical quenching. A response to excess light energy. Plant Physiol 125:1558–1566. https://doi.org/10.1104/pp.125.4.1558

Müller MG, Lambrev P, Reus M et al (2010) Singlet energy dissipation in the photosystem II light-harvesting complex does not involve energy transfer to carotenoids. ChemPhysChem 11:1289–1296. https://doi.org/10.1002/cphc.200900852

Park S, Fischer AL, Li Z et al (2017) Snapshot transient absorption spectroscopy of carotenoid radical cations in high-light-acclimating thylakoid membranes. J Phys Chem Lett 8:5548–5554. https://doi.org/10.1021/acs.jpclett.7b02486

Park S, Fischer AL, Steen CJ et al (2018) Chlorophyll-carotenoid excitation energy transfer in high-light-exposed thylakoid membranes investigated by snapshot transient absorption spectroscopy. J Am Chem Soc 140:11965–11973. https://doi.org/10.1021/jacs.8b04844

Park S, Steen C, Lyska D, Fischer AL (2019) Chlorophyll-carotenoid excitation energy transfer and charge transfer in *Nannochloropsis oceanica* for the regulation of photosynthesis. Proc Natl Acad Sci USA 116:3385–3390

Pascal AA, Liu Z, Broess K et al (2005) Molecular basis of photoprotection and control of photosynthetic light-harvesting. Nature 436:134–137. https://doi.org/10.1038/nature03795

Polívka T, Sundström V (2004) Ultrafast dynamics of carotenoid excited states—from solution to natural and artificial systems. Chem Rev 104:2021–2071

Porra RJ, Thompson WA, Kriedemann PE (1989) Determination of accurate extinction coefficients and simultaneous equations for assay in chlorophylls a and b extracted with four different solvents. Biochim Biophys Acta 975:384–394

Ruban AV, Berera R, Ilioaia C et al (2007) Identification of a mechanism of photoprotective energy dissipation in higher plants. Nature 450:575–578. https://doi.org/10.1038/nature06262

Sacharz J, Giovagnetti V, Ungerer P et al (2017) The xanthophyll cycle affects reversible interactions between PsbS and light-harvesting complex II to control non-photochemical quenching. Nat Plants. https://doi.org/10.1038/nplants.2016.225

Staleva H, Komenda J, Shukla MK et al (2015) Mechanism of photoprotection in the cyanobacterial ancestor of plant antenna proteins. Nat Chem Biol 11:287–291. https://doi.org/10.1038/nchembio.1755

Sylak-Glassman EJ, Zaks J, Amarnath K et al (2016) Characterizing non-photochemical quenching in leaves through fluorescence lifetime snapshots. Photosynth Res 127:69–76. https://doi.org/10.1007/s11120-015-0104-2

Vieler A, Wu G, Tsai CH et al (2012) Genome, functional gene annotation, and nuclear transformation of the heterokont oleaginous alga *Nannochloropsis oceanica* CCMP1779. PLoS Genet. https://doi.org/10.1371/journal.pgen.1003064

Wahadoszamen M, Margalit I, Ara AM et al (2014) The role of charge-transfer states in energy transfer and dissipation within natural and artificial bacteriochlorophyll proteins. Nat Commun 5:1–8. https://doi.org/10.1038/ncomms6287

Wang H, Whittaker-Brooks L, Fleming GR (2015) Exciton and free charge dynamics of methylammonium lead iodide perovskites are different in the tetragonal and orthorhombic phases. J Phys Chem C 119:19590–19595. https://doi.org/10.1021/acs.jpcc.5b04403

Werley CA, Teo SM, Nelson KA (2011) Pulsed laser noise analysis and pump-probe signal detection with a data acquisition card. Rev Sci Instrum. https://doi.org/10.1063/1.3669783

Wilson KS, Wong CY (2018) In situ measurement of exciton dynamics during thin-film formation using single-shot transient absorption. J Phys Chem A 122:6438–6444. https://doi.org/10.1021/acs.jpca.8b06248